The effects of composition, temperature and annealing on the rheological properties of InZn *in situ* composites

Samuel P. Balch and Roderic S. Lakes

July 25, 2016

Department of Engineering Physics, University of Wisconsin-Madison, Madison, WI 53706, USA

Adapted from Balch, S. and Lakes, R. S., "The effects of composition, temperature, and annealing on the rheological properties of InZn in situ composites", Rheologica Acta, 55, (4), 335-341 (2016).

Abstract

High viscoelastic damping is observed in InZn materials over ranges of composition, frequency, temperature and annealing time. Microscopy reveals InZn when cast segregates into a heterogeneous micro-structure resembling an *in situ* composite consisting of a zinc matrix with soft indium platelet inclusions. This morphology is predicted to be advantageous for maximizing the damping figure of merit $Etan\delta$ by viscoelastic composite theory. InZn is found to be linearly viscoelastic, unlike other high damping metals. The damping of InZn varies little over a substantial range of temperature, in contrast with polymers. For 5% In material, the optimal composition, $Etan\delta$ is 2.8 GPa at 10 Hz, compared to a peak of 0.6 GPa for high damping rubbers. After annealing for 13 years, $Etan\delta$ was still high at 1.9 GPa. InZn demonstrates high damping under a wide range of conditions.

keywords: Complex modulus, Dynamic mechanical properties, Linear viscoelasticity, Solid, Structure, Dynamic moduli

1 Introduction

Materials that are stiff and have high, linearly viscoelastic damping are of practical interest to solve noise and vibration problems in machinery and structures. Tuned dampers and layered surface damping treatments are common solutions to reduce or eliminate noise and vibrations that rely on viscoelastic materials. For vibration of plates or bars, the figure of merit for effective damping is the product of the modulus of elasticity and the tangent of the material phase angle ($Etan\delta$), shown by [Cremer et al.(1988)]. Conventional materials are limited to an $Etan\delta$ less than 0.6 GPa [Lakes(2009), chap. 7]. Viscoelastic materials with better performance could lead to lighter and less bulky damping solutions for aerospace, automotive, naval and other applications.

Polymer damping layers are commonly used. They provide a maximum $Etan\delta$ of 0.6 GPa. However, this performance is only available when the polymer is in the transition region between rubbery and glassy response. Thus, polymer damping performance is highly sensitive to temperature and the frequency of vibration.

In contrast to polymers, high damping metals also provide structural rigidity. Several varieties are available. The zinc-aluminum alloys commonly used in die casting, studied by [Ritchie et al.(1991)], exhibit high damping at low frequencies and high temperature but only provide a $Etan\delta$ of less than 0.1 GPa above 1000 Hz at room temperature. Sonoston, a copper-manganese alloy, is used as high damping material in naval propellers. [Ritchie et al.(1985)] demonstrated Sonoston is non-linearly viscoelastic and the high damping capacity is only available at large strain, limiting it to high amplitude applications. Nickel-titanium shape memory alloys can have high damping over a range of temperatures but they were also shown to be non-linearly viscoelastic by [Hasiguti and Iwasaki(1968)]. High damping composites consisting of tungsten and cadmium laminae were found to have high damping by [Brodt and Lakes(1995)], but these laminates are dense and anisotropic.

ZnAl-SiC composites were lighter and also provided high damping [Jaglinski and Lakes (2012)]. High stiffness and damping over a narrow range of temperature were obtained in composites with barium titanate inclusions [Jaglinski et al. (2007)]; constrained negative stiffness of the inclusions were responsible for the effect. Initial study InZn material with 5% indium over 8.5 decades of frequency revealed high damping at ambient temperature [Balch and Lakes (2015)]. These materials all entail a high degree of contrast in properties between the heterogeneities and the matrix.

A material that is macroscopically homogeneous and isotropic with a high $Etan\delta$ over a wide range of frequency and temperature would have broad appeal for applications in noise and vibration suppression. Too, insensitivity to annealing time in comparison with polymers can be beneficial for applications in which materials are in service for prolonged use. In the present study, the rheological properties of four compositions of indium-zinc material are evaluated.

2 Materials and Methods

2.1 Materials Selection

Indium and zinc were selected as constituents because (i) they have little mutual solubility, and (ii) zinc is stiff (E = 100 GPa) and has high damping for a metal; indium has higher damping (and is more compliant. A mixture of indium and zinc will segregate into two phases, one consisting of 99.9%-100% zinc and another consisting of 98%-100% indium, as indicated by the phase diagram given by [Dutkiewicz and Zakulski(1984)]. As a molten mixture of indium and zinc cools, the zinc rich phase precipitates out of the liquid first, then the indium rich phase solidifies. This forms an *in situ* composite with a stiff, high damping matrix of zinc and soft indium inclusions.

2.2 Specimen Preparation

The specimens evaluated in this study were prepared by mixing indium and zinc in solid state, melting the mixture in a borosilicate glass and rapidly cooling the mixture. This was done in

an effort to evenly disperse the phases to achieve an isotropic material.

The solid state mixing was done using a hot press to make a sandwich of zinc wafers and indium pieces then folding the sandwich and pressing again. Two pure zinc pieces were cut from an ingot of 99.9% pure zinc obtained from Alfa Aesar. A Carver press with a heated cylinder was used to press the zinc into thin disks. The flattened disks were massed and the amount of indium required for the desired composition was calculated.

The indium was 99.99% pure, tear drop shaped shot obtained from Alfa Aesar. The soft shot was cut into small pieces with a utility knife. The correct mass of these indium pieces was placed between the zinc disks and pressed into a wafer. The wafer was folded in half and pressed. This was repeated until the metals appeared mixed, about five times. The wafer was massed after every fold to ensure no material was lost.

After folding and pressing, the wafer was cut into small pieces. The pieces were put into a borosilicate glass specimen tube with an inner diameter of 3.2 mm. The specimen tube was closed on one end, the other end was sealed with a short steel rod. The specimen tube was placed in a larger glass tube with one closed end for handling.

A Fisher Scientific Isotemp® Muffle Furnace was heated to 480°C. The handling tube was placed in the furnace horizontally. After three minutes, the tube was removed from the furnace, tapped on a soft piece of foam for compaction, spun horizontally for mixing and placed back into the furnace. This was repeated every five minutes. When the specimen was fully melted and mixed, the tube was removed and spun horizontally in air at room temperature while it cooled and solidified.

The specimen tube was removed from the outer tube. The specimen was freed by cracking the specimen tube in a vice. This produced a cylindrical specimen about 50mm in length, 3.2mm in diameter and 3.5g of mass. The upper end was contaminated with soot and the lower end came to a point due to the shape of the closed end of the specimen tube. Test specimens were made by cutting off the ends of the cylinder with a Buehler IsoMet® 1000 precision saw with a diamond blade. This low speed, wet saw cuts the material without affecting its material properties.

Specimens with 5%, 15%, 50% and 85% indium were prepared and tested in this study. Some were subject to preliminary tests, then annealed at room temperature for 13 years; others were prepared and tested after 14 weeks annealing time.

2.3 Experimental Overview

The viscoelastic properties of the specimens were measured over a broad range of frequency. All compositions were tested in the sub-audible and audible range of frequency with broadband viscoelastic spectroscopy in torsion. Specimens with promising performance, the 5% and 15% indium specimens, were tested at ultrasonic frequencies using resonant ultrasonic spectroscopy and wave ultrasound.

The structure of the 5% indium specimen was observed using optical and scanning electron microscopy.

2.4 Broadband Viscoelastic Spectroscopy (BVS)

Broadband viscoelastic spectroscopy (BVS), discussed in detail by [Brodt et al.(1995)], is a method of testing the viscoelastic properties of a specimen from creep to ultrasonic frequencies. In BVS, a slender rod shaped specimen is attached to a support rod in fixed-free end conditions. The support rod is connected to a massive stiff hollow brass cylinder which forms the test chamber of the instrument. Instrument compliance is reduced to insignificance by making the support rod much stiffer than the specimen.

A strong permanent magnet is bonded to the free end of the specimen. Torque is applied to the specimen through the interaction of the permanent magnet and a uniform magnetic field produced by a Helmholtz coil. Orthogonal coils allow the specimen to be tested in bending and torsion. In this study, torsion was used. For

dynamic studies, a signal generator is used to provide an alternating current to the Helmholtz coil which generates a sinusoidal torque on the specimen. The magnet is calibrated by mounting it on a specimen of a known material and calculating the amount of torque applied from the modulus of the known material.

The response of the specimen to the torque is measured optically. A laser beam is directed into the test chamber and onto a mirror attached to the magnet. The laser reflects out of the chamber onto a New Focus 2901 quadcell photo-detector, which is mounted on a micrometer driven translation stage. The photo-detector converts the lateral position of the reflected beam to a voltage. It is calibrated by moving the stage a known amount and observing the difference in voltage.

With a sinusoid torque input at a frequency below the first resonant mode of the specimen, the dynamic shear modulus is determined by comparing the input sinusoid, from which torque is inferred, and the output sinusoid (produced by the photo-detector) from which angular displacement is inferred. The sinusoids are characterized using a Stanford Research Systems SR-850 lock-in amplifier. The structural phase angle (φ) is found by subtracting the torque signal's phase angle (ϕ_τ) from the angle signal's phase angle (ϕ_θ), shown in equation 1.

$$\varphi = \phi_\theta - \phi_\tau \tag{1}$$

A dynamic correction is applied to the structural phase angle (φ) to find the material phase angle (δ), equation 2, where ν is the frequency of the measurement and ν_0 is the first resonant frequency of the specimen.

$$tan\delta = tan\varphi \left[1 - \left(\frac{\nu}{\nu_0}\right)^2\right] \tag{2}$$

The magnitude of the dynamic shear modulus is calculated via equation 3:

$$|G^*| = \frac{MV_\tau}{R_{fb}}\ell \Big/ \left[\frac{\pi}{32}d^4 tan^{-1}\left(\frac{V_\theta}{2KD}\right)\right] \tag{3}$$

where M is the calibration constant of the magnet, V_τ is the RMS magnitude of the torque signal, R_{fb} is the feedback resistance [1], ℓ is the length of the specimen, d is the diameter of the specimen, V_θ is the RMS magnitude of the angle signal, K is the calibration constant of the photo-detector and D is the distance from the specimen mirror to the photo-detector.

Near and above the first resonant frequency, the above relations are no longer valid. However, the material damping can be found by measuring the quality factor (Q) of a resonant peak. This is done by scanning frequencies to find resonant peaks. When a peak is found, its magnitude and frequency (ν_0) are recorded and the frequencies lower and higher than the peak are found such that the magnitude of the response is half the magnitude of the peak (ν_L and ν_H). From this, the Q is found and $tan\delta$ is approximately the inverse of Q, shown in equation 4.

$$tan\delta \approx Q^{-1} = \frac{\nu_H - \nu_L}{\sqrt{3}\nu_0} \tag{4}$$

The temperature of the measurement is controlled by blowing conditioned air into the testing chamber. Temperature is monitored by placing thermocouples in the air flow very close to specimen. Thermocouples are placed at the bottom and top on specimen to monitor temperature gradient.

2.5 Resonant Ultrasonic Spectroscopy (RUS)

Resonant ultrasonic spectroscopy (RUS) [Demarest(1971)]; [Migliori and Maynard(2005)] via shear transducers [Wang and Lakes(2002)], was used to expand the test frequency range and corroborate the BVS results of the 5% and 15% indium specimens. RUS is a method of measuring elastic and viscoelastic properties using broadband ultrasonic transducers. The specimen is cut into a shape such as a cube or short cylinder which has an analytical solution for the first resonant mode. The specimen is excited by the one transducer and its response is measured by another transducer. The frequency of excitation is scanned until the first natural frequency is found. The

[1] Used to scale torque signal which allows a wide variety of specimens from very compliant to very stiff.

magnitude of the shear modulus of a short cylinder is given by equation 5, which follows from the analytical solution for the lowest natural frequency of a cylinder in free-free end conditions. In equation 5, ν_0 is the first natural frequency, ρ is the density of the material, and ℓ is the length and diameter of the cylinder.

$$|G^*| = (2\nu_0\ell)^2\rho \tag{5}$$

Damping is inferred from the quality factor of the resonant peak. This is done via equation 4, exactly the same is in BVS.

2.6 Wave Ultrasound

To determine the attenuation of the 5% and 15% indium specimens, ultrasonic testing is used. A Panametrics 500 PR pulse-receiver is used to generate a broadband pulse, which is transmitted to the specimen using an ultrasonic transducer. The pulse is received on the other end of the specimen with another transducer. The pulse delay and magnitude of the return are recorded. Equation 6 gives the attenuation (α). Further experiments are done using tone bursts from a Tektronix function generator with the aim of exploring possible resonances of the micro-structure.

$$A_1 = A_0 e^{-\alpha z} \tag{6}$$

In equation 6, A_1 is the amplitude of the received signal, z is the length of the specimen and A_0 is a constant. Attenuation is found by varying the length of the specimen and fitting equation 6 to the data.Shear transducers are used for measurements at 5 MHz and longitudinal transducers are used for 10 MHz. The attenuation of shear waves can be different than the attenuation of longitudinal waves in the same material.

Attenuation is related to $tan\delta$ by equation 7, where phase velocity (c) is calculated from the pulse delay and ν is the frequency of the pulses.

$$\alpha \approx \frac{\pi\nu}{c} tan\delta \tag{7}$$

The pulse-receiver excites the transmitting transducer at the transducer's natural frequency. Different transducers can be used to find the attenuation at different frequencies. The magnitude of the dynamic shear modulus is found with equation 8 when shear transducers are used.

$$c = \sqrt{\frac{|G^*|}{\rho}} \tag{8}$$

2.7 Microscopy

A specimen for optical microscope study was cut from the end of a BVS test specimen using an IsoMet® 1000 saw. For optical microscopy, the specimen was mounted in epoxy, ground with graded abrasives and polished with colloidal silica. Next, the specimen was etched with a 10% solution of hydrochloric acid and water and polished once more. A Olympus BH2-1 microscope with a digital camera and QCapture Pro 6.0 image acquisition software was use to create micrographs.

The composition of these phases was verified using energy dispersive x-ray spectroscopy in an LEO 1530 scanning electron microscope (SEM). SEM specimens were ground and polished but not etched to preserve the chemical composition of the surface.

3 Experimental Results

Four compositions of indium-zinc materials were tested with BVS at room temperature; 5%, 15%, 50% and 85%. A summary of the results can be found in table 1.

Table 1: BVS results at 10 Hz, pure zinc data from [Wang et al.(2004)].

Composition	**Age**	$\|\mathbf{G}^*\|$	**tan**δ	**Etan**δ
pure zinc	unknown	46 GPa	1%	1.2 GPa
5% indium	14 weeks	29.6 GPa	3.61%	2.8 GPa
5%	13 years	34.5 GPa	2.04%	1.9 GPa
15%	13 years	21.1 GPa	3.13%	1.8 GPa
50%	13 years	12.3 GPa	5.24%	1.7 GPa
85%	13 years	7.15 GPa	5.77%	1.1 GPa

As the indium content increases, the stiffness is reduced while the loss tangent increases. In

table 1, E was calculated from G using the Poisson's ratio of zinc. The 5% and 15% indium specimens have nearly the same performance $Etan\delta$ at low frequency.

As the frequency increases into the audible range, the loss tangent of the 5% indium specimen stays steady while the other compositions loss tangents decrease significantly, shown in figure 1.

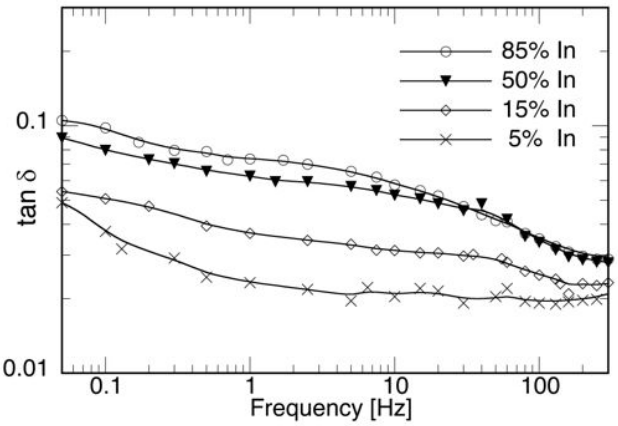

Figure 1: Loss tangent of specimens annealed 13 years and measured with BVS at sub-resonant frequencies.

While the loss tangent in all except the 5% indium specimen decreases substantially with increasing frequency, the stiffness of all specimens increases modestly, shown in figure 2.

Figure 3 shows the stiffness and damping of the 5% and 15% indium specimens over a wide range of frequency, from sub audible to ultrasonic. At ultrasonic frequencies, both specimens exhibit strong attenuation. At 10 MHz, the 5% attenuates at 840 nepers per meter and 15% attenuates at 750 nepers per meter. Studies via tone bursts from 0.7 to 3.0 MHz at closely spaced frequencies revealed no sharp anomalies indicative of any resonance of the microstructure.

The newer specimen's viscoelastic properties were measured at a range of temperatures from 0°C to 80°C. Figure 4 shows that damping monotonically increases and modulus monotonically decreases a modest amount with temperature.

By contrast, the $tan\delta$ curve for commercial polymer damping layers has a sharp peak that is

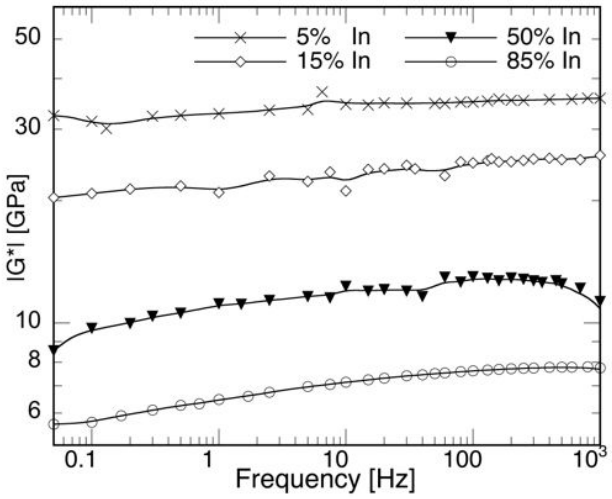

Figure 2: Shear modulus of specimens annealed 13 years and measured with BVS at sub-resonant frequencies.

only about 20°C wide at half maximum [Capps and Beumel(1990

As the material annealed, it became stiffer and damped less.

The 5% indium specimen was studied with optical microscopy to reveal the structure and electron microscopy to confirm the composition of the phases observed optically.

In figure 6, the grain structure of the material is shown. The grains are the zinc rich phase and the indium rich phase is found in the grain boundaries.

Figure 7 is an image of a grain taken using the backscattered electron channel of the SEM. In this channel, atoms with higher atomic numbers appear lighter than atoms with lower atomic numbers. Indium, atomic number 49, appears white. Zinc, atomic number 30 appears grey.

4 Theory and Discussion

Two analytical models of isotropic composite materials can be applied to this material; the Hashin-Shtrikman model for composites arbitrary phase geometry and the analytical solution for composites with dilute, thin, soft, randomly oriented platelet inclusions [Christensen(1979)]. Hashin-Shtrikman provides the upper and lower bounds

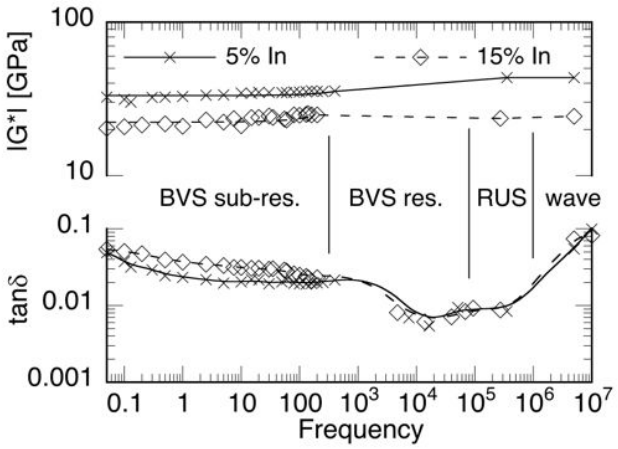

Figure 3: Loss tangent and shear modulus of 5% and 15% indium specimens annealed 13 years and measured at room temperature across a wide range of frequency using methods indicated in figure.

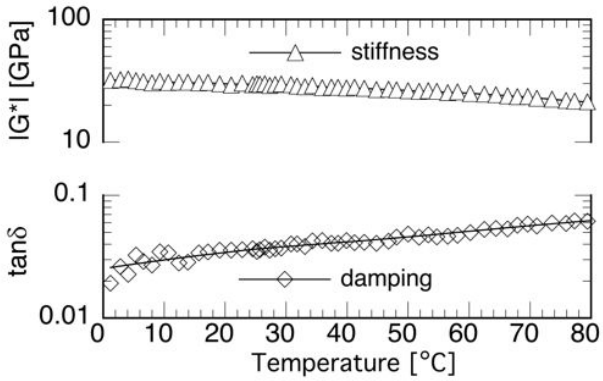

Figure 4: Loss tangent and shear modulus of 5% indium specimen annealed 14 weeks and measured with BVS at 10 Hz across a range of temperature.

of stiffness and the dilute platelet model provides the exact stiffness. The structure revealed in the micrographs most resembles composite consisting of a zinc matrix and dilute, randomly oriented, platelet shaped indium inclusions.

Predictions of stiffness of elastic isotropic composites can be applied to viscoelastic composites via the correspondence principle [Lakes(2009), chap. 9]. If harmonic loading is assumed, complex dynamic moduli simply can be substituted for static (real) moduli. The dynamic shear modulus consists of real and imaginary components, $G^* = G' + iG''$. This can be resolved into the magnitude of the dynamic shear modulus, $|G^*|$ and the loss tangent, the ratio of the real and imaginary parts: $tan\delta = G'/G''$.

When the correspondence principle is applied, the upper bound of the dynamic modulus of the Hashin-Shtrikman model is given by equation 9 and lower bound is given by equation 10, from [Chen and Lakes(1993)]. In equations 9, 10 and 11, K^* is the dynamic bulk modulus, V is the volume fraction and the subscripts refer the constituents of the composite.

$$G_U^* = G_1^* + V_2 \Big/ \left[\frac{1}{G_2^* - G_1^*} + \frac{6V_1(K_1^* + 2G_1^*)}{5G_1^*(3K_1^* 4G_1^*)}\right] \tag{9}$$

$$G_L^* = G_2^* + V_1 \Big/ \left[\frac{1}{G_1^* - G_2^*} + \frac{6V_2(K_2^* + 2G_2^*)}{5G_2^*(3K_2^* 4G_2^*)}\right] \tag{10}$$

The analytical solution for the dynamic modulus of the dilute platelet model is shown in equation 11, also from [Chen and Lakes(1993)].

$$G^* = G_1^* + \frac{V_2(G_2^* - G_1^*)}{15}\left[\frac{9K_2^* + 4G_1^* + 8G_2^*}{K_2^* + \frac{4}{3}G_2^*} + \frac{6G_1^*}{G_2^*}\right] \tag{11}$$

Figure 8 shows the Hashin-Shtirkman bounds and dilute platelet solution of stiffness and damping for an indium-zinc composite material plotted at various compositions. The experimental results at 1 Hz dynamic loading are shown.

The newer 5% indium specimen has good agreement with the dilute platelet model while the older specimen behaves as if it has a lower concentration of platelets. This annealing behavior may be due to diffusion of indium into quenched-in vacancies in the zinc grains, effectively reducing the concentration of platelets. The 15% indium material has poor agreement with the dilute platelet model because it's structure

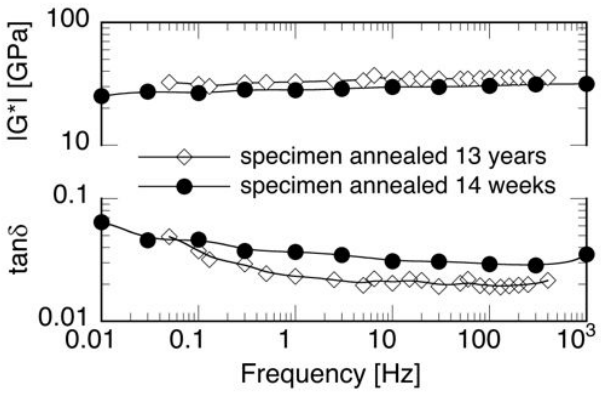

Figure 5: Loss tangent and shear modulus of 5% indium specimens annealed 14 weeks and 13 years measured with BVS at room temperature across a range of frequency.

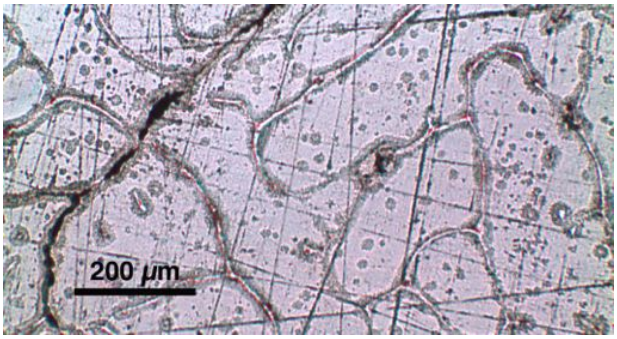

Figure 6: Optical microscope image of 5% indium specimen at 10x magnification.

is less like the dilute platelet model, which assumes thin platelets.

The damping effect in both phases is likely due to dislocation drag at high homologous melting temperature. At room temperature, indium and zinc are at 69% and 43% of the homologous melting temperature, respectively. This is why damping increases and stiffness decreases steadily with increasing temperature.

As for annealing, glassy polymers are known to exhibit substantial annealing (or physical aging) effects [Hodge(1995)] after they are polymerized. The rate of aging in glassy polymers depends in part upon how far below the glass transition temperature T_g the polymer is used. Because commercial polymer damping layers are used at temperatures in the vicinity of T_g, more

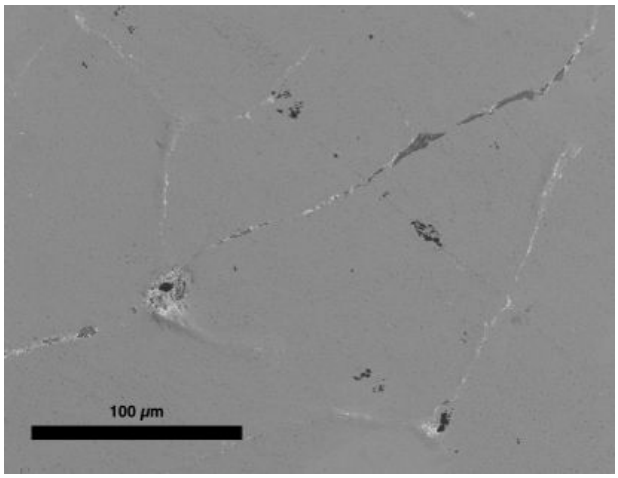

Figure 7: SEM image of grain from back scattered electron channel.

rapid aging is expected. Physical aging in polymers may be due to evaporation of plasticizer in plasticized material or from molecular rearrangement in glassy polymers. In glassy polymers the effect of aging is represented by a shift of the creep curves along the log time axis. For example in a PVC polymer, a factor of ten in aging time slowed creep curves by about a factor of eight on the time scale. In damping applications, such a shift would substantially reduce the damping. The change in properties of InZn after prolonged annealing is modest in comparison with that of polymers.

Indium-zinc *in situ* composite has potential as a structural damping material or as a damping layer that contributes structural stiffness. For example, it could be used as a die-casting material that provides high vibration damping over a wide range of temperatures and frequencies. Engine mounts cast from indium-zinc could lead to quieter cars through operating temperature and engine speed envelopes. Machinery noise shields could be thinner or more effective if indium-zinc is used as the damping layer.

Indium-zinc could be used as the matrix material for a low density composite with silicon carbide or with barium titanate. This would effectively form a three phase composite, a topic for further study.

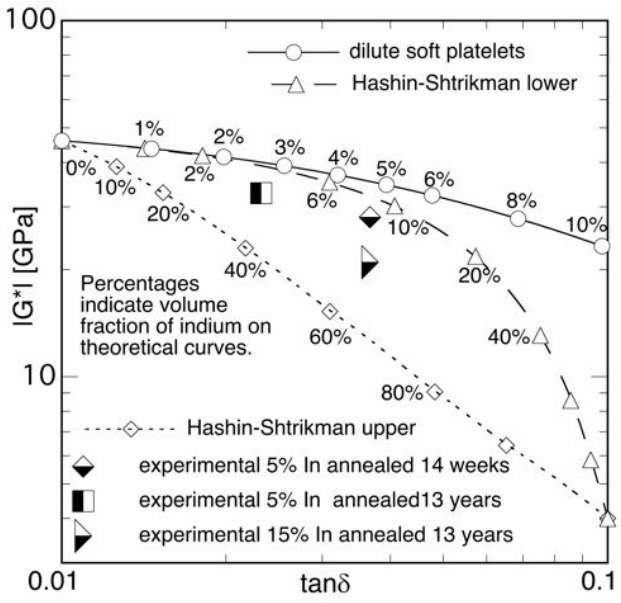

Figure 8: Hashin-Shtrikman and dilute soft platelet composite theory extended to viscoelastic material and compared to experimental results.

5 Conclusions

Indium-zinc *in situ* composite provides high damping figure of merit over a wide frequency range from sub-audio to ultrasonic. For the optimal composition 5% In, $Etan\delta$ is 2.8 GPa at 10 Hz. This is higher than a peak of 0.6 GPa for high damping rubbers. High damping is maintained over a considerable range of temperature and also following prolonged annealing.

6 acknowledgements

Support from the Army Research Office is gratefully acknowledged.

References

[Balch and Lakes (2015)] Balch, S and Lakes, RS (2015) High vibration damping in in situ In-Zn composites, Functional Materials Letters, 8, (5) 1550059

[Brodt et al.(1995)] Brodt M, Cook LS, Lakes RS (1995) Apparatus for measuring viscoelastic properties over ten decades: refinements. Rev of Sci Instrum 66:5292-5297

[Brodt and Lakes(1995)] Brodt M, Lakes RS (1995) Composite materials which exhibit high stiffness and high viscoelastic damping. J of Compos Mater 29:1823-1833

[Capps and Beumel(1990)] Capps RN, Beumel LL (1990) Dynamic mechanical testing, application of polymer development to constrained layer damping. In: Corsaro RD, Sperling LH (eds) Sound and vibration damping with polymers. American Chemical Society, Washington DC, pp 63-78

[Chen and Lakes(1993)] Chen CP, Lakes RS (1993) Analysis of high loss viscoelastic composites. J of Mater Sci 28:4299-4304

[Christensen(1979)] Christensen RM (1979) Mechanics of composite materials. John Wiley and Sons, New York, pp 107-151

[Cremer et al.(1988)] Cremer L, Heckl M, Ungar EE (1988) Structure- borne sound, 2nd edn. Springer-Verlag, Berlin, pp 245

[Demarest(1971)] Demarest RD Jr. (1971) Cube-resonance method to determine the elastic constants of solids, J of Acoust Soc of Am 49:768-775.

[Dutkiewicz and Zakulski(1984)] Dutkiewicz J, Zakulski W (1984) The In-Zn (indium-zinc) system. Bull of Alloy Phase Diagr 5:284-289

[Hasiguti and Iwasaki(1968)] Hasiguti RR, Iwasaki K (1968) Internal friction and related properties of the TiNi intermetallic compound. J of Appl Phys 39:2182-2186

[Hodge(1995)] Hodge I (1995) Physical aging in polymeric glasses, Sci 267:1945-1947

[Jaglinski and Lakes (2012)] Jaglinski TM, Lakes RS (2012) Zn-Al based metal matrix composites with high stiffness and high viscoelastic damping. J of Compos Mater 46:755-763

[Jaglinski et al. (2007)] Jaglinski TM, Kochmann D, Stone D, Lakes RS (2007) Materials with viscoelastic stiffness greater than diamond, Sci 315:620-622

[Lakes(2009)] Lakes R (2009) Viscoelastic materials. Cambridge University Press, New York, pp 209-270

[Migliori and Maynard(2005)] Migliori A, Maynard JD (2005) Implementation of a modern resonant ultrasound spectroscopy system for the measurement of the elastic moduli of small solid specimens, Rev of Sci Instrum 76:121301

[Ritchie et al.(1991)] Ritchie IG, Pan ZL, Goodwin FE (1991) Characterization of the damping properties of die-cast zinc-aluminum alloys. Metal Trans A 22A:617-622

[Ritchie et al.(1985)] Ritchie I, Sprungmann K, Sahoo M (1985) Internal friction in Sonoston - a high damping Mn/Cu-based alloy for marine propeller applications. J de Phys Colloq 46:C10-409 - C10-412

[Wang and Lakes(2002)] Wang YC, Lakes RS (2002) Resonant ultrasound spectroscopy in shear mode, Rev of Sci Instrum 74:1371-1373

[Wang et al.(2004)] Wang YC, Ludwigson M, Lakes RS (2004) Deformation of extreme viscoelastic metals and composites. Mater Sci and Eng A 379:41-49